International Journal of Nanomedicine

Dovepress
open access to scientific and medical research

Open Access Full Text Article

ORIGINAL RESEARCH

Strategy for chemotherapeutic delivery using a nanosized porous metal-organic framework with a central composite design

This article was published in the following Dove Press journal:
International Journal of Nanomedicine
22 February 2017
Number of times this article has been viewed

Yingpeng Li[1]
Xiuyan Li[2]
Qingxia Guan[2]
Chunjing Zhang[2]
Ting Xu[2]
Yujing Dong[2]
Xinyu Bai[2]
Weiping Zhang[3]

[1]College of Pharmacy, Tianjin University of Traditional Chinese Medicine, Tianjin, [2]College of Pharmacy, Heilongjiang University of Traditional Chinese Medicine, Harbin, People's Republic of China; [3]Pope John XXIII High School, Everett, MA, USA

Background: Enhancing drug delivery is an ongoing endeavor in pharmaceutics, especially when the efficacy of chemotherapy for cancer is concerned. In this study, we prepared and evaluated nanosized HKUST-1 (nanoHKUST-1), nanosized metal-organic drug delivery framework, loaded with 5-fluorouracil (5-FU) for potential use in cancer treatment.

Materials and methods: NanoHKUST-1 was prepared by reacting copper (II) acetate [$Cu(OAc)_2$] and benzene-1,3,5-tricarboxylic acid (H_3BTC) with benzoic acid (C_6H_5COOH) at room temperature (23.7°C±2.4°C). A central composite design was used to optimize 5-FU-loaded nanoHKUST-1. Contact time, ethanol concentration, and 5-FU:material ratios were the independent variables, and the entrapment efficiency of 5-FU was the response parameter measured. Powder X-ray diffraction, scanning electron microscopy (SEM), transmission electron microscopy (TEM), and nitrogen adsorption were used to determine the morphology of nanoHKUST-1. In addition, 5-FU release studies were conducted, and the in vitro cytotoxicity was evaluated.

Results: Entrapment efficiency and drug loading were 9.96% and 40.22%, respectively, while the small-angle X-ray diffraction patterns confirmed a regular porous structure. The SEM and TEM images of the nanoHKUST-1 confirmed the presence of round particles (diameter: approximately 100 nm) and regular polygon arrays of mesoporous channels of approximately 2–5 nm. The half-maximal lethal concentration (LC_{50}) of the 5-FU-loaded nanoHKUST-1 was approximately 10 μg/mL.

Conclusion: The results indicated that nanoHKUST-1 is a potential vector worth developing as a cancer chemotherapeutic drug delivery system.

Keywords: 5-fluorouracil, drug delivery, nanoparticles, nano-MOFs

Introduction

Despite encouraging progress in cancer therapeutics over the past 30 years, cancer remains to be the most intractable disease entity in this century.[1] Conventional chemotherapeutic agents, in whatever novel ways they could work,[2,3] have not competently circumvented a major challenge in oncology, the drug resistance. In addition, most of these antineoplastic agents act by targeting tumor cells through a somewhat specific approach,[4] and are therefore compromised by a dose window and a toxicity profile. To achieve better tumor eradication, a treatment strategy for cancer, known as nanoparticle (NP) therapy, is now being developed using nanotechnology.

NP therapy has been recognized by the National Cancer Institute to cause a revolution in modern medicine for the detection, treatment, and prevention of cancers.[5] NPs target tumor features to deliver chemotherapeutic agents selectively and specifically. A considerable number of NP formulations for drug delivery have been explored,

Correspondence: Xiuyan Li
College of Pharmacy, Heilongjiang University of Traditional Chinese Medicine, Heping Road 24, Harbin, Heilongjiang Province, People's Republic of China
Tel/fax +86 451 8726 6893
Email lixiuyan211486@163.com

submit your manuscript | www.dovepress.com
Dovepress
http://dx.doi.org/10.2147/IJN.S119115

including liposomes,[6] dendrimers,[7] nanotubes,[8] polymeric biodegradable NP nanocapsules,[9] and metal-organic frameworks (MOFs).[10]

Traditional MOFs are hybrid materials made from metal ion connectors and polydentate bridging ligands that have been exploited in bulk scale for versatile applications including gas adsorption,[11–17] catalysis,[18–20] nonlinear optics,[21] separation,[22,23] magnetism,[24,25] chemical sensors,[26–28] and drug delivery.[29,30] Compared with other types of drug delivery NPs, the advantages of MOFs include simple preparation, high specific surface area, and excellent porosity. The high structural flexibility of certain porous MOFs may also enable the adaptation of their porosity into the shape of host molecules.[31,32] Horcajada et al reported that the compounds MIL-100 and MIL-101 have a good loading capacity for Ibuprofen, which can be released slowly under physiological conditions.[33]

One of the milestone products of MOFs was HKUST-1 developed by Chui et al from the Hong Kong University of Science and Technology in 1999,[34] using copper (Cu) as the metal connector because it is a trace element required for human health, and benzene tricarboxylic acid (H_3BTC) as the bridging ligand for better stability. HKUST-1 $[Cu_3(BTC)_2(H_2O)_3]_n$ was prepared by reacting trimesic acid and copper nitrate at a 1:1 ratio for 12 h at a temperature of 180°C. The specific area and pore volume were 692.2 m^2/g and 0.333 cm^3/g, respectively. It had a three-dimensional network structure composed of a $[Cu_2(O_2CR)_4]$ (paddle-wheel) secondary structure unit with a 9×9 Å square hole. It had a high thermal stability and did not decompose at 240°C. Then, the free water in the pores was removed by vacuum drying at 150°C to reveal the coordinated unsaturated metal active center, which functionally modified the framework.[34] However, traditional MOFs were still large, which compromised their transfection efficiency.

Recently, nano-MOFs (NMOFs) with a much smaller particle size based on NPs of nontoxic porous organic carboxylic acid coordination polymers were shown to exhibit important drug-loading characteristics, progressive release, and imaging properties.[29,33,35,36] Furthermore, the method for preparing the nanosized HKUST-1 (nanoHKUST-1) involved titrimetry at room temperature. Therefore, it is of interest to formulate nanoHKUST-1 encapsulating a common chemotherapeutic agent as host drug and evaluate the release of nano-encapsulated drug in an exploratory study.

5-Fluorouracil (5-FU) could be a suitable host drug for such studies because its molecular size is small enough to be encapsulated in the nanoHKUST-1 cavity.[37] Although widely used in the treatment of gastrointestinal, breast, ovarian, and cervical cancers, 5-FU is well documented for its structural instability and multi-organ adverse effects.[38–43] We hypothesized that nanoHKUST-1-encapsulated 5-FU may show better anticancer actions with less biotoxicity and more steady release.

The aim of the present research study was to develop an NMOF sustained-release system for 5-FU. This paper describes the preparation and characterization of nanoHKUST-1, in vitro release kinetics of the drug from 5-FU-loaded nanoHKUST-1, and the in vitro cytotoxicity of nanoHKUST-1 and 5-FU-loaded nanoHKUST-1.

Materials and methods

Materials

All the chemicals used in this study were of analytical grade. N,N-Dimethylformamide (DMF) (Tianjin Standard Chemical Reagent Co., Ltd., Tianjin, People's Republic of China), copper (II) acetate $[Cu(OAc)_2]$ and benzoic acid (C_6H_5COOH; both from Guangfu Chemical Industry Co., Ltd., Tianjin, People's Republic of China), and H_3BTC (Henghua Technology Co., Ltd., Jinan, People's Republic of China) were used to prepare the nanoHKUST-1.

Preparation of HKUST-1

First, $Cu(OAc)_2$ (0.3 g) and benzoic acid C_6H_5COOH (4 g) as a modulator were dissolved in 30 mL normal butyl alcohol. Then, H_3BTC (0.8 g) was dissolved in 30 mL DMF and stirred, and this mixture was added dropwise to the metal salt solution $[Cu(OAc)_2]$ slowly at room temperature (25°C) over a period of 30 min. A blue sediment was observed during the addition of H_3BTC, and the solution was stirred for 30 min. The resultant NMOFs were recovered by centrifugation (10,000 rpm), and the solvent was removed along with the residual non-reacted organic acids by washing twice with ethanol.

Characterization

The powder X-ray diffraction (PXRD) analysis was performed using a Phillips Xpert Pro MPD diffractometer with Cu Kα radiation (λ=1.5418 nm) at 40 kV and 50 mA. The nitrogen adsorption was measured using an MFA-140 (Beijing Builder Electronic Technology Co., Ltd., Beijing, People's Republic of China), and the samples were activated for 4 h at 120°C before the measurements. The surface area was calculated using the Brunauer–Emmett–Teller (BET) model. The transmission electron microscopy (TEM) and scanning electron microscopy (SEM) images were obtained

using a JEM-2100 JEOL and a Quanta 200F (FEI Sirion SEM), respectively. Differential scanning calorimetry (DSC) was performed using WCT-1D (Beijing Optical Century Instrument Co., Ltd., Beijing, People's Republic of China).

Preparation of SEM samples

The conductive adhesive was cut into small pieces and glued onto the aluminum foil. The crushed samples were smeared on the conductive adhesive using a toothpick or cotton swab and then sprayed on the gold samples. The accelerating voltage was 15–30 kV, and magnification was 40,000–80,000 times.

Preparation of TEM samples

The samples were dissolved in absolute alcohol, and small samples were dropped on the microgrid and dried under natural air.

The DSC was performed under the following conditions: nitrogen flow, 20 mL/min; temperature range, 0°C–450°C; heating rate, 10°C/min; and duration, 40 min. We weighed 10 mg samples accurately and placed them close to the bottom of the crucible, which was placed into the instrument. The temperature was subsequently recorded to construct the curves.

Encapsulation

For the encapsulation studies, the nanoHKUST-1 was vacuum-dried at 150°C for 16 h, and suspended in freshly prepared 5-FU in ethyl alcohol, and the suspension was stirred for several days at room temperature. The 5-FU-loaded NPs were then collected by centrifugation and vacuum-dried at room temperature.

Central composite design of 5-FU-loaded nanoHKUST-1

In this study, a central composite design was used to optimize the 5-FU-loaded nanoHKUST-1. Before using this design, some preliminary experiments were conducted. We had discovered that the 5-FU encapsulation efficiency was related to contact time, ethanol concentration, and 5-FU-to-nanoHKUST-1 ratios. Therefore, these variables were selected as independent variables. The effects of these variables were studied at three experimental levels: 1, 0, and −1. The actual and coded values for the different variables are shown in Table 1. Three formulations of the 5-FU-loaded nanoHKUST-1 were designed to optimize the experimental parameters (Table 2), and the entrapment efficiency of 5-FU in the test formulations was used as a response parameter.

Table 1 Actual values of independent variables

X	Variables	Units	−1	0	1
X_1	Contact time	h	48	72	96
X_2	Ethanol concentration	%	70	80	90
X_3	5-FU:material ratio	None	5	6	7

Abbreviation: 5-FU, 5-fluorouracil.

Entrapment efficiency and drug loading

To measure the 5-FU loading using high-performance liquid chromatography (HPLC), 5 mg dried 5-FU-loaded nanoHKUST-1 was treated with ultrasonic waves for 30 min with ethanol as an extraction reagent. We used a Dimma ODS-C_{18} (200×4.6 mm, 5 μm) column under the following conditions: mobile phase, methanol:water (20:80); flow rate, 1 mL/min; column temperature, 30°C; and injective volume, 10 μL. An ultraviolet detector was used at a wavelength of 266 nm. Then, the 5-FU encapsulation efficiency was calculated as the percentage of drug that was effectively entrapped inside the NPs compared to the total drug used in the preparation procedure.

In vitro release

The objective of the in vitro release test was to predict the in vivo effects. Therefore, the conditions for in vitro release were required to simulate the in vivo conditions as much as possible. The experimental methods and conditions were also required to meet the correlation between the body and the exterior environment. Presently, the commonly used methods for the determination of in vitro release are the classical,

Table 2 Formulation of 5-FU-loaded nanoHKUST-1 using central composite design

Run	X_1	X_2	X_3	Drug loading (%)
1	1	0	−1	9.56
2	−1	0	−1	11.40
3	0	−1	−1	8.63
4	1	−1	0	16.58
5	1	0	1	16.01
6	1	1	0	8.75
7	0	0	0	7.02
8	0	0	0	6.47
9	0	1	−1	11.00
10	0	−1	1	14.16
11	−1	−1	0	10.40
12	0	0	0	10.33
13	−1	0	1	12.80
14	0	1	1	10.11
15	−1	1	0	9.28
16	0	0	0	5.47
17	0	0	0	4.68

Abbreviations: 5-FU, 5-fluorouracil; nanoHKUST-1, nanosized HKUST-1.

dialysis, chamber diffusion, and the flow cell methods. We used the dialysis method in this study.

The 5-FU release from the nanoHKUST-1 was analyzed using dialysis bags (Sigma-Aldrich, St Louis, MO, USA) pre-soaked in double-distilled water for 12 h. The freeze-dried 5-FU-loaded NP suspensions were placed into the dialysis bags, which were submerged in 50 mL phosphate-buffered saline (pH 7.4) to maintain sink conditions. The dialysis preparations were shaken at 100 rpm in a constant-temperature shaker (SHAB; Donglian Electric Technique Co., Ltd., Harbin, People's Republic of China) at 37°C. Subsequently, 2 mL of the release medium was withdrawn at regular intervals, and fresh release medium was added to maintain a constant volume. Every trial was repeated three times. The samples were then analyzed using HPLC, while the control experiments were similarly performed using the same proportions to investigate the drug release.

In vitro cytotoxicity studies

The human hepatocellular carcinoma (HepG2) cell lines (Beijing Boyu Kangtai International Biological Technology Co., Ltd., Beijing, People's Republic of China) used in this experiment were maintained in Roswell Park Memorial Institute-1640 medium (Hyclone; Thermo Fisher Scientific, Inc., Waltham, MA, USA) supplemented with 10% heat-inactivated fetal calf serum (Sijiqing Tianhang Biological Science and Technology Co., Ltd., Hangzhou, People's Republic of China), 10^5 U/L penicillin G, and 100 mg/L streptomycin in 7.5 cm^2 tissue culture flasks in a humidified atmosphere of 5% CO_2 and 37°C.

The cells were plated in 96-well flat-bottomed microtiter plates, and 5-FU (7.8–1,000 μg/mL) was added to the complete cell culture medium. Then, eight concentrations each of the empty nanoHKUST-1 and 5-FU-nanoHKUST-1 were prepared (7.8–1,000 μg/mL). After 48-h incubation, the chemosensitivity was evaluated using the thiazolyl blue tetrazolium bromide (MTT reagent, 98%; Sigma-Aldrich) in complete cell culture medium (5 μg/mL). Then, 20 μL of the MTT reagent was added to each well and incubated for 4 h, and the mitochondrial aldehyde dehydrogenase from the viable cells subsequently reduced the yellow soluble MTT reagent to water-insoluble blue formazan crystals, which were dissolved by adding 200 μL dimethyl sulfoxide to each well. The absorbance of the dissolved formazan blue dye was measured at 492 nm using an automated multiscan ascent 7000 microplate reader (Thermolab Electron Co., Dreiereich, Germany), and the cell viability calculations were performed as follows:

$$\text{Cell inhibition rate (\%)} = 1 - \frac{A_E - A_B}{A_C - A_B} \times 100,$$

where A_E, A_B, and A_C are the experimental, blank, and control group values, respectively. Each concentration was repeated in six wells.

Results

Structure and morphology

The PXRD patterns including the small-angle X-ray diffraction (XRD) patterns are shown in Figure 1. Specifically, Figure 1A shows a small peak at 2°–3°, which confirms a regular porous structure. The small peak between 2° and 3° disappeared after loading the drug, which indicates that the

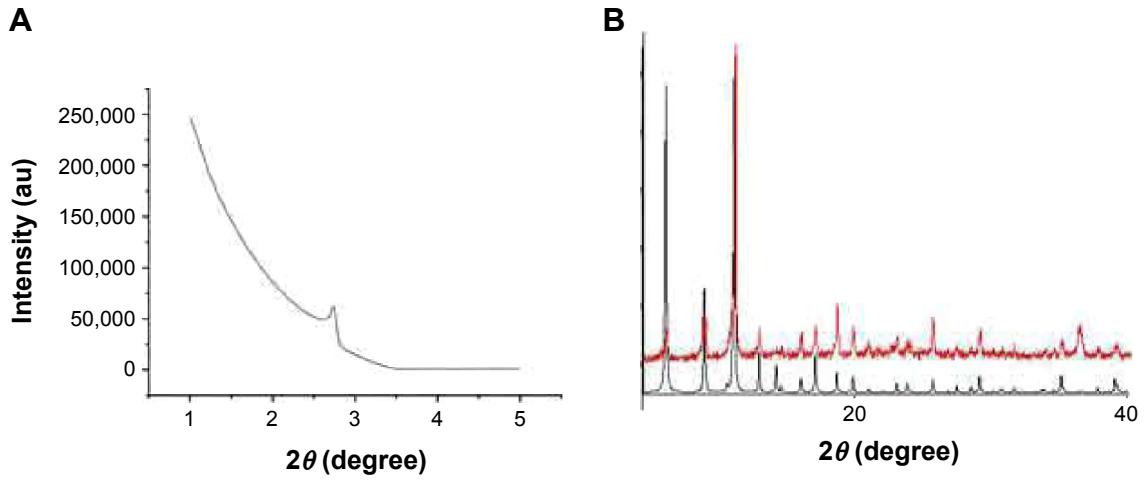

Figure 1 Low-angle and wide-angle XRD spectra of nanoHKUST-1.
Notes: (**A**) Low-angle XRD spectra of nanoHKUST-1. Small peak at 2–3 indicates internal regular porous structure, which confirms sample was a porous material. (**B**) Wide-angle XRD spectra of nanoHKUST-1. XRD patterns of synthetic nanoHKUST-1 (black) and standard HKUST-1 (red). XRD patterns of sample show same peaks as those of standard, which confirms the high purity of nanoHKUST-1. Peaks patterns of sample account for rough appearance of nanosized particles.
Abbreviations: XRD, X-ray diffraction; nanoHKUST-1, nanosized HKUST-1.

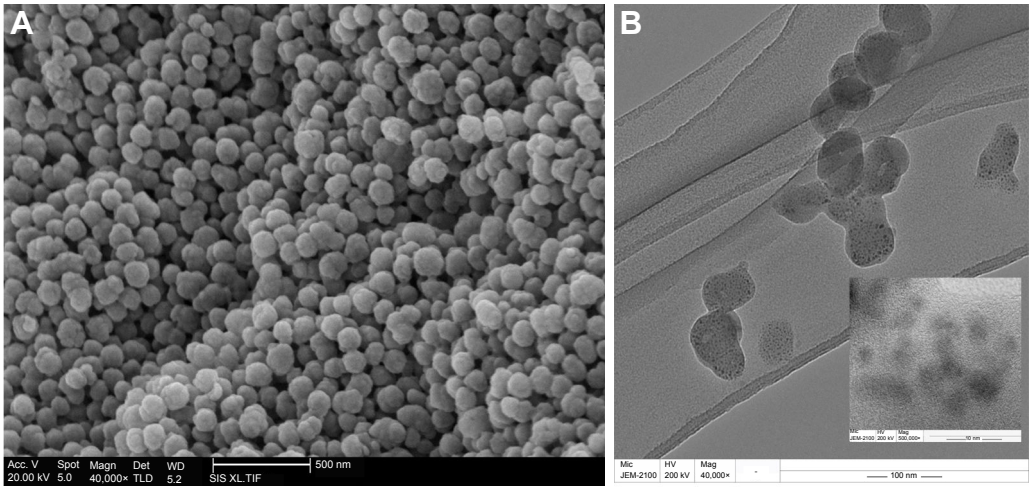

Figure 2 SEM and TEM images of morphology of nanoHKUST-1.
Notes: (**A**) SEM images of morphology of nanoHKUST-1. Particles show regular round, uniform distribution, with no adhesion and a size of 50–100 nm. Single-particle surface is rough, indicating existence of pores. (**B**) TEM images of morphology of nanoHKUST-1 showing a pore diameter of 2–5 nm. The white part of the inset in B is pore canal, and the black part is pore wall.
Abbreviations: SEM, scanning electron microscopy; TEM, transmission electron microscopy; nanoHKUST-1, nanosized HKUST-1.

drugs were incorporated into the channels. The wide-angle XRD patterns in Figure 1B illustrate that the HKUST-1 materials possess three well-resolved peaks, similar to the standard patterns.

The SEM and TEM images of the HKUST-1 are shown in Figure 2, and the sample consisted of round particles (diameter: approximately 100 nm). The TEM images show regular polygon arrays of mesoporous channels and pore diameters of approximately 2–5 nm.

The nitrogen gas (N_2) adsorption–desorption isotherms and pore size distribution of HKUST-1 are shown in Figure 3. The isotherms had a broad hysteresis loop of 0.2–0.9 (Figure 3A), confirming that it was a mesoporous material. The pore size distribution curves in Figure 3B indicate an average pore size of 2 nm, while a broad peak at 10 nm indicates the distance between the particles. The BET surface area was 227 m^2/g, and the pore volume was 0.61 cm^3/g.

The 5-FU-loaded nanoHKUST-1 were prepared according to the formulation factors predicted by the central composite design. The SEM image of the 5-FU-loaded nanoHKUST-1 is shown in Figure 4, which indicates that the particles were not destroyed during drug loading. The DSC result illustrated in Figure 5 shows the similarity of the

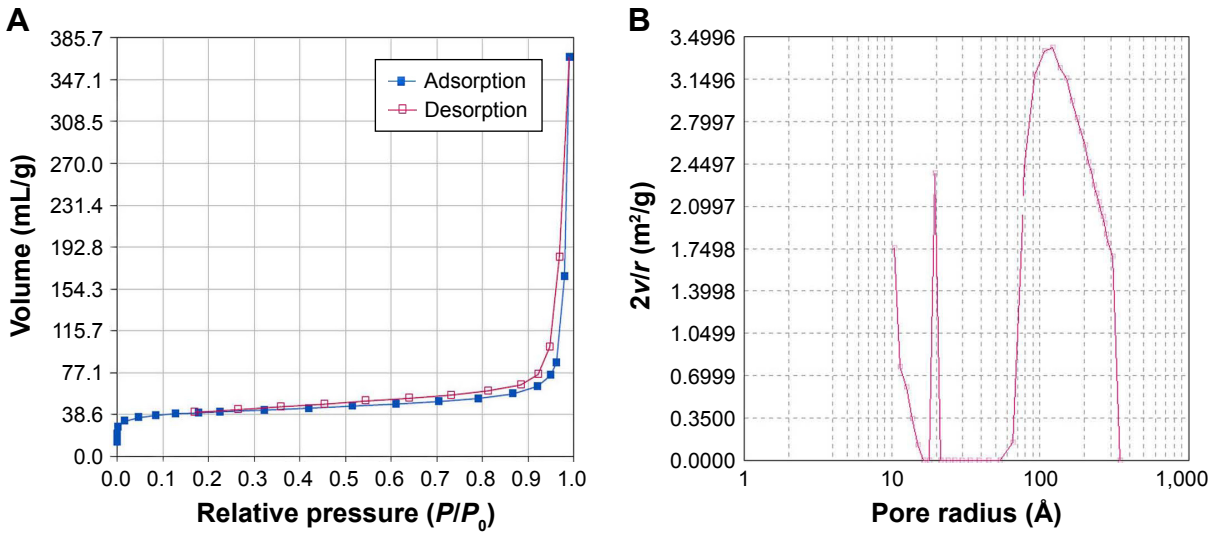

Figure 3 Nitrogen adsorption–desorption isotherms and pore size distribution of HKUST-1.
Notes: (**A**) Nitrogen adsorption–desorption isotherms. Hysteresis loop phenomenon appears in the range of relative high pressure, indicating the existence of channels in sample. (**B**) BJH pore size distributions. First peak shows average pore size was approximately 2–5 nm. Peak approximately 10 nm wide was caused by interstitial pore generated by accumulation of particles. *P* refers to liquid nitrogen saturation vapour pressure; P_0 refers to equilibrium vapour pressure; *v* refers to pore volume; *r* refers to pore radius.
Abbreviation: BJH, of Barrett-Joyner-Halenda.

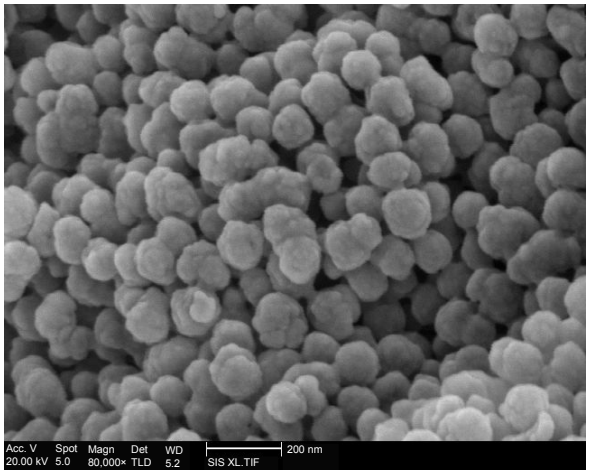

Figure 4 SEM images of morphology of 5-FU-loaded nanoHKUST-1. Morphological structure of carriers was not obviously changed compared with that of drug-loaded carriers.
Abbreviations: SEM, scanning electron microscopy; 5-FU, 5-fluorouracil.

curves obtained before and after drug loading, which began to collapse at 337.5°C, while that of 5-FU was destroyed at 272°C. There were no corresponding peaks in the 5-FU-loaded nanoHKUST-1 at 272°C. This may be because the 5-FU was encapsulated in the nanoHKUST-1 channels and the heat generated may have been offset by both components. The drug-loading process proved to have no effect on the thermal stability of nanoHKUST-1.

HPLC analysis

The standard curve for 5-FU was drawn (linear regression equation for 5-FU: $y = 3{,}226{,}692x - 20{,}238.3$ and R^2=0.9997), and a good linear relationship was observed between the peak areas and concentrations.

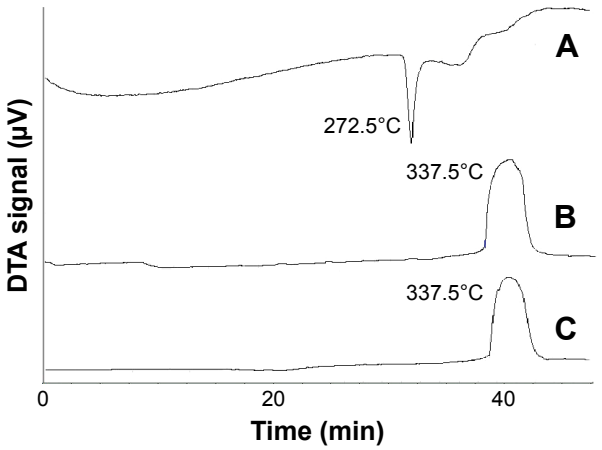

Figure 5 DSC patterns.
Notes: Patterns of (**A**) 5-FU, (**B**) nanoHKUST-1, and (**C**) 5-FU-loaded nanoHKUST-1. Result shows curves before and after drug loading were similar and began to decompose at 337.5°C, while 5-FU decomposed at 272°C. Drug-loading process proved to have no effect on thermal stability of nanoHKUST-1.
Abbreviations: DSC, differential scanning calorimetry; 5-FU, 5-fluorouracil; nanoHKUST-1, nanosized HKUST-1; DTA, differential thermal analysis.

Optimization of formulations and statistical analysis

The central composite design was used with the aim of studying the factor variables by fitting the effect variables, which could make up for the deficiency of the uniform and orthogonal design. Therefore, it was expected to facilitate the analysis of the interaction between the experimental factors, ensure the accuracy of the test, and require less experimental time. Data from the central composite design were analyzed using the Design-Expert software, version 8.0.6. The polynomial equation fitting to the data is depicted in Table 3, and the model was highly statistically significant (R=0.9165, $P<0.05$), with a statistically insignificant lack of fit ($P>0.05$). The interactions of the three factors were not significant ($P<0.05$). The influence of the ratio of 5-FU to desolvated nanoHKUST-1 (X_3) was higher than that of the other factors. The following polynomial equation gave the final equation in terms of actual factors:

$$\begin{aligned}\text{Drug loading (\%)} = {} & 6.79 + 0.88 \times X_1 - 1.33 \times X_2 + 1.56 \\ & \times X_3 - 1.68 \times X_1 \times X_2 + 1.26 \times X_1 \\ & \times X_3 - 1.61 \times X_2 \times X_3 + 2.96 \times X_1^2 \\ & + 1.50 \times X_2^2 + 2.69 \times X_3^2\end{aligned}$$

where X_1 represents the contact time, X_2 represents the ethanol concentration, and X_3 represents the ratio of 5-FU to desolvated nanoHKUST-1.

A three-dimensional map is shown in Figure 6, and here, the adsorbed 5-FU increased with the initial

Table 3 ANOVA results

Source	Sum of squares	*df*	Mean square	*F* value	*P*-value probability > *F*
Model	152.64	9	16.96	4.08	0.0385
X_1	6.16	1	6.16	1.48	0.2627
X_2	14.12	1	14.12	3.40	0.1077
X_3	19.50	1	19.50	4.70	0.0669
X_1X_2	11.26	1	11.26	2.71	0.1437
X_1X_3	6.38	1	6.38	1.54	0.2552
X_2X_3	10.30	1	10.30	2.48	0.1592
X_1^2	36.97	1	36.97	8.90	0.0204
X_2^2	9.42	1	9.42	2.27	0.1758
X_3^2	30.37	1	30.37	7.31	0.0304
Residual	29.07	7	4.15		
Lack of fit	10.18	3	3.39	0.72	0.5905
Pure error	18.88	4	4.72		
Core total	181.71	16			

Abbreviation: ANOVA, analysis of variance.

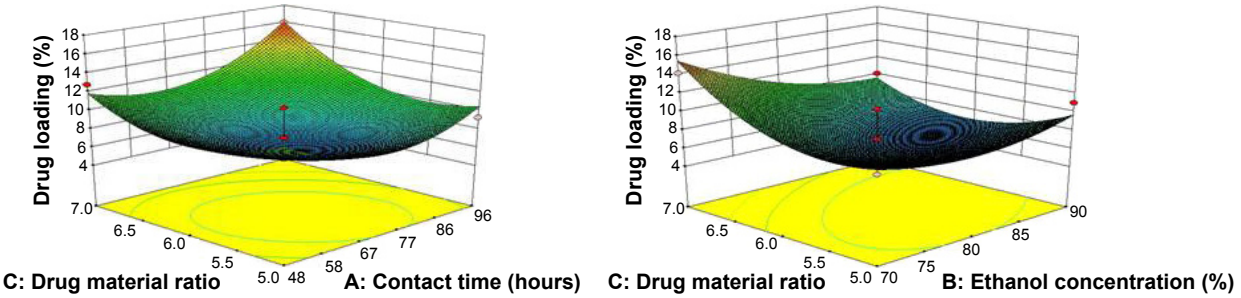

Figure 6 Three-dimensional map of X_1 (contact time), X_2 (ethanol concentration), and X_3 (5-FU:nanoHKUST-1 ratios) after interaction of independent variables. Optimized ethanol concentration was 70%, drug-loading ratio was 7:1, and delivery time was 96 h.
Abbreviations: 5-FU, 5-fluorouracil; nanoHKUST-1, nanosized HKUST-1.

5-FU:material ratios expressed in weight and optimal value (7:1), corresponding to a maximum solubility of 5-FU in 80% ethanol. The maximal adsorption was obtained after 4 days. Therefore, the best results were achieved when the desolvated nanoHKUST-1 was immersed for 4 days in a 14 mg/mL 5-FU-ethanol solution with a 5-FU:desolvated HKUST-1 weight ratio of 7:1. Finally, the optimized total entrapment efficiency and drug loading were determined as 9.96% and 40.22%, respectively, which were greater than the 5-FU loading previously reported in polyethylene glycol (PEG) (15%).[44,45]

In vitro release

Figure 7 shows the release profiles of 5-FU from the nanoHKUST-1, which indicates a relative burst drug release. In contrast to the non-encapsulated drug formulations, there was a pronounced prolongation of the drug release from the nanoHKUST-1. While approximately 90% of the non-encapsulated drug was found in the release medium, only 60% of the drug was released from NPs after approximately 10 h. In the literature, plenty of theoretical or empirical release models are described.[46,47] Zero- and first-order kinetics, as well as Higuchi models, have been used to evaluate the release of encapsulated drugs. The first-order kinetic equation was $y = 18.25 \times \ln(x) + 10.09$ (r^2=0.9823). The release of 5-FU from the nanoHKUST-1 fitted a sustained-release first-order model.

In vitro cytotoxicity studies

In contrast to the 5-FU-treated cells, the inhibition of $HepG_2$ cells treated with 5-FU-loaded nanoHKUST-1 increased in a dose-dependent manner (Figure 8). The half-maximal lethal concentration (LC_{50}) values of nanoHKUST-1, 5-FU, and the 5-FU-loaded nanoHKUST-1 were calculated to be 72.75, 74.00, and 5.66 µg/mL, respectively. In summary, the 5-FU-loaded nanoHKUST-1 at the observed LC_{50} values

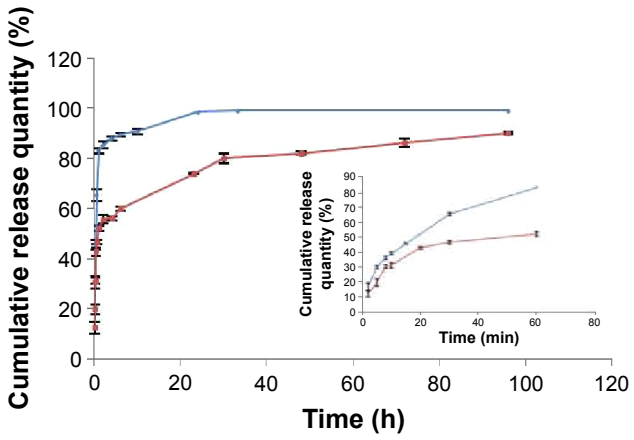

Figure 7 In vitro release curves for 5-FU (blue line) and 5-FU-loaded nanoHKUST-1 (red line). After approximately 10 h, 90% of 5-FU was found in release medium, while only 60% of drug was released from NPs. Every trial was repeated three times. All values are shown as mean ± SD.
Abbreviations: 5-FU, 5-fluorouracil; NPs, nanoparticles; SD, standard deviation; nanoHKUST-1, nanosized HKUST-1.

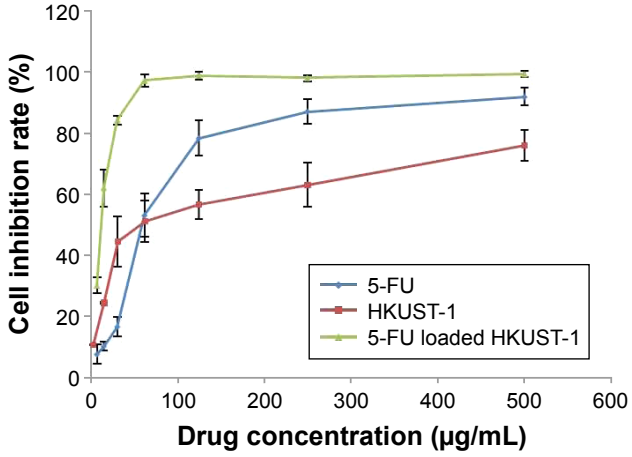

Figure 8 Comparison of cytotoxicities of 5-FU, empty nanoHKUST-1, and 5-FU-loaded nanoHKUST-1 using MTT assay. Toxicity of nanoHKUST-1 was lowest, while that of 5-FU-loaded nanoHKUST-1 was highest. Each concentration was repeated in six wells. All values are shown as mean ± SD.
Abbreviations: 5-FU, 5-fluorouracil; SD, standard deviation; nanoHKUST-1, nanosized HKUST-1.

decreased the viability of the $HepG_2$ cells compared to the 5-FU treatment ($P<0.05$).

Discussion

The effects of NMOFs on drug delivery carriers have attracted considerable attention from researchers over the past several decades.[30,48–50] NMOFs have been used for the loading and controlled release of various drugs for their large surface area and pore size. Compared to other carriers, the nanoHKUST-1 has a rapid adsorption rate, high loading efficiency, and low drug release rate.

The structure of the empty nanoHKUST-1 was confirmed as a nanosized porous material using PXRD. The peak shape was rough because of the smaller particle size, while no obvious peak was observed. In addition, the diffraction peaks were observed at a range of $2\theta < 1°$ for both the square and round particles, proving that the formulated nanoHKUST-1 was a highly ordered nanomaterial.

The BET surface areas and micropore volume of the nanoHKUST-1 were determined using the N_2 adsorption isotherms, which showed it was a microporous material. The N_2 adsorption method is a common method used to determine the specific surface area and pore size of nanomaterials. The determination principle of N_2 adsorption is that the surface pore of the porous materials will absorb nitrogen at the temperature of liquid nitrogen. The flat areas on the low-pressure section were caused by the nanopores. The N_2 adsorption quantity increased suddenly, which caused the hysteresis loop, indicating the existence of micropores, and this phenomenon was caused by capillary condensation. The pore diameter distribution revealed the average pore diameter to be 2–5 nm, while there was a wide peak of approximately 10 nm, which was caused by the larger pore size of the particles. The SEM and TEM showed that the carriers had a uniform size and round structure, while the high surface area and hollow space enabled them to efficiently load more drugs.

The drug-loading efficiency (DLE) depended on the drug particles and the pore size of the framework. 5-FU,[51] which has a small particle size, penetrated the pores of the nanoHKUST-1. From the encapsulation experiment, we discovered that the nanoHKUST-1 loaded more drugs than most of the carriers such as PEG (15%, $P<0.05$). We produced three batches of the 5-FU-loaded nanoHKUST-1 according to the optimal preparation, and their DLE was 40.23%, 34.58%, and 38.43%, respectively (standard deviation: 2.89, $P>0.05$). This observation proved that the optimized process was stable and reproducible.

The structural characteristics of the 5-FU-loaded nanoHKUST-1 were evaluated using DSC and SEM. The SEM images showing the morphology of 5-FU-loaded nanoHKUST-1 indicate that the embedding of the drug did not affect the framework morphology. The differential thermal analysis curve proved that the samples were still heat-stable after the drug-loading process. The interactions between the drug and the carriers were caused by a supramolecular relationship.[52]

Numerous factors could affect or enhance the release of the 5-FU from the particles including desorption of the drug adsorbed on the sphere surface, diffusion of drug through the sphere, and erosion of the sphere.[53] The drug release curve showed that the drug burst occurred at the first half an hour. The release rate of 5-FU-loaded nanoHKUST-1 was 52% at the first few hours, and this was caused by the diffusion of the drug adsorbed on the surface of the carriers into the release medium. The release of 5-FU in this system offered two dose release levels. The first was an immediate-release dose, which produced the desired pharmacological effect, while the second was a maintenance dose that prolonged the duration of the pharmacological response.[52] Questions may arise as to whether the duration of the initial burst release can be controlled, and whether it would be possible to prepare the formulation which takes less time for the drug to reach a desired concentration in the bloodstream. We speculated that these could be achieved by reducing the drug adsorbed on the surface of the carriers, or by coating with a layer of multi-polymer outside the carriers. Future studies are warranted to address these problems.

Human hepatocellular carcinoma HepG2 cells are derived from human fetal liver cells. The biological transformation of the enzyme is homologous to the human normal liver parenchyma cells. HepG2 also performs some functions as normal liver cells do, and is widely available in pharmaceutical laboratories. Moreover, HepG2 is not rigorously environment-demanding for its growth. Since its establishment, it has become an important cell line for screening and studying the pathogenesis of liver cancer.[54–57] The MTT assay demonstrated the cytotoxicity of the 5-FU-loaded nanoHKUST-1. NanoHKUST-1 at low concentration (15 μg/mL) showed slight inhibition (24.3%), which was the same as that of the 5-FU-solution (10.2%). In contrast, the 5-FU-loaded nanoHKUST-1 killed almost half of the cells (62.0% inhibition rate), which was much higher than that of 5-FU and nanoHKUST-1 ($P<0.05$). From these results, it was concluded that nanoHKUST-1 at a low concentration (<15 μg/mL) have a good safety profile in HepG2 cells.

These results were similar to those obtained with zinc nanoscale MOFs (IRMOF-3), which did not significantly affect the morphology, viability, and membrane integrity of the cells at concentrations <25 μg/mL.[58] A limitation should be acknowledged that the present study was not complete as it did not explore the cytotoxicity of these formulations in a healthy non-cancer cell line because we primarily focused on whether the MOF could achieve a larger drug loading and reduce drug release. Subsequent studies on the cytotoxicity of 5-FU-loaded nanoHKUST-1 on cancer vs normal cells would therefore be interesting.

Conclusion

Based on the results of this study, 5-FU incorporated into the nanoHKUST-1 appeared to be a useful tool for the treatment of cancer because of its enhanced encapsulation efficiency and controlled release of drug from the nanocarriers. Our future studies should be focused on elucidating the activity of the NMOF drug delivery system and its effects on the mechanism of action of the encapsulated anticancer drug.

Acknowledgments

The authors would like to thank the teachers and students of the College of Pharmacy of Heilongjiang University of Traditional Chinese Medicine for their contributions to this study. This work was supported by the College of Pharmacy, Heilongjiang University of Traditional Chinese Medicine (grant no 2014bs06) and National Natural Science Foundation of China (NSFC) (grant no. 404G041).

Author contributions

All authors contributed toward data analysis, drafting and critically revising the paper and agree to be accountable for all aspects of the work.

Disclosure

The authors report no conflicts of interest in this work.

References

1. Chen W, Zheng R, Zeng H, Zhang S, He J. Annual report on status of cancer in China, 2011. *Chin J Cancer Res*. 2015;27(1):2–12.
2. Youns M, Hoheisel JD, Efferth T. Therapeutic and diagnostic applications of nanoparticles. *Curr Drug Targets*. 2011;12(3):357–365.
3. Rahman M, Ahmad MZ, Kazmi I, et al. Advancement in multifunctional nanoparticles for the effective treatment of cancer. *Expert Opin Drug Deliv*. 2012;9(4):367–381.
4. Akhter S, Ahmad I, Ahmad MZ, et al. Nanomedicines as cancer therapeutics: current status. *Curr Cancer Drug Targets*. 2013;13(4):362–378.
5. Anand P, Sundaram C, Jhurani S, Kunnumakkara AB, Aggarwal BB. Curcumin and cancer: an "old-age" disease with an "age-old" solution. *Cancer Lett*. 2008;267(1):133–164.
6. Batra H, Antony VB. Pleural mesothelial cells in pleural and lung diseases. *J Thorac Dis*. 2015;7(6):964–980.
7. Maeng JH, Lee DH, Jung KH, et al. Multifunctional doxorubicin loaded superparamagnetic iron oxide nanoparticles for chemotherapy and magnetic resonance imaging in liver cancer. *Biomaterials*. 2010;31(18):4995–5006.
8. Sinha N, Yeow JT. Carbon nanotubes for biomedical applications. *IEEE Trans Nanobioscience*. 2005;4(2):180–195.
9. Kedar U, Phutane P, Shidhaye S, Kadam V. Advances in polymeric micelles for drug delivery and tumor targeting. *Nanomedicine*. 2010;6(6):714–729.
10. Cherukuri P, Glazer ES, Curley SA. Targeted hyperthermia using metal nanoparticles. *Adv Drug Deliv Rev*. 2010;62(3):339–345.
11. Yaghi OM, O'Keeffe M, Ockwig NW, Chae HK, Eddaoudi M, Kim J. Reticular synthesis and the design of new materials. *Nature*. 2003;423(6941):705–714.
12. Evans OR, Lin W. Crystal engineering of NLO materials based on metal – organic coordination networks. *Acc Chem Res*. 2002;35(7):511–522.
13. Wu CD, Hu A, Zhang L, Lin W. A homochiral porous metal-organic framework for highly enantioselective heterogeneous asymmetric catalysis. *J Am Chem Soc*. 2005;127(25):8940–8941.
14. Férey G, Mellot-Draznieks C, Serre C, Millange F. Crystallized frameworks with giant pores: are there limits to the possible? *Acc Chem Res*. 2005;38(4):217–225.
15. Chen B, Zhao X, Putkham A, et al. Surface interactions and quantum kinetic molecular sieving for H2 and D2 adsorption on a mixed metal-organic framework material. *J Am Chem Soc*. 2008;130(20):6411–6423.
16. Sumida K, Rogow DL, Mason JA, et al. Carbon dioxide capture in metal-organic frameworks. *Chem Rev*. 2012;112(2):724–781.
17. Suh MP, Park HJ, Prasad TK, Lim DW. Hydrogen storage in metal-organic frameworks. *Chem Rev*. 2012;112(2):782–835.
18. Cho SH, Ma B, Nguyen ST, Hupp JT, Albrecht-Schmitt TE. A metal-organic framework material that functions as an enantioselective catalyst for olefin epoxidation. *Chem Commun (Camb)*. 2006;(24):2563–2565.
19. Jiang HL, Xu Q. Porous metal-organic frameworks as platforms for functional applications. *Chem Commun (Camb)*. 2011;47(12):3351–3370.
20. Yoon M, Srirambalaji R, Kim K. Homochiral metal-organic frameworks for asymmetric heterogeneous catalysis. *Chem Rev*. 2012;112(2):1196–1231.
21. Liu Y, Li G, Li X, Cui Y. Cation-dependent nonlinear optical behavior in an octupolar 3D anionic metal-organic open framework. *Angew Chem Int Ed Engl*. 2007;46(33):6301–6304.
22. Li JR, Sculley J, Zhou HC. Metal-organic frameworks for separations. *Chem Rev*. 2012;112(2):869–932.
23. Li JR, Kuppler RJ, Zhou HC. Selective gas adsorption and separation in metal-organic frameworks. *Chem Soc Rev*. 2009;38(5):1477–1504.
24. Kurmoo M. Magnetic metal-organic frameworks. *Chem Soc Rev*. 2009;38(5):1353–1379.
25. Shen L, Yang SW, Xiang S, et al. Origin of long-range ferromagnetic ordering in metal-organic frameworks with antiferromagnetic dimeric-Cu(II) building units. *J Am Chem Soc*. 2012;134(41):17286–17290.
26. Kreno LE, Leong K, Farha OK, Allendorf M, Van Duyne RP, Hupp JT. Metal-organic framework materials as chemical sensors. *Chem Rev*. 2012;112(2):1105–1125.
27. Bétard A, Fischer RA. Metal-organic framework thin films: from fundamentals to applications. *Chem Rev*. 2012;112(2):1055–1083.
28. Lu ZZ, Zhang R, Li YZ, Guo ZJ, Zheng HG. Solvatochromic behavior of a nanotubular metal-organic framework for sensing small molecules. *J Am Chem Soc*. 2011;133(12):4172–4174.
29. Sun CY, Qin C, Wang XL, Su ZM. Metal-organic frameworks as potential drug delivery systems. *Expert Opin Drug Deliv*. 2013;10(1):89–101.
30. Dekrafft KE, Boyle WS, Burk LM, Zhou OZ, Lin W. Zr- and Hf-based nanoscale metal-organic frameworks as contrast agents for computed tomography. *J Mater Chem*. 2012;22(35):18139–18144.

31. Férey G, Serre C. Large breathing effects in three-dimensional porous hybrid matter: facts, analyses, rules and consequences. *Chem Soc Rev*. 2009;38(5):1380–1399.
32. Das MC, Xiang S, Zhang Z, Chen B. Functional mixed metal-organic frameworks with metalloligands. *Angew Chem Int Ed Engl*. 2011;50(45):10510–10520.
33. Horcajada P, Chalati T, Serre C, et al. Porous metal-organic-framework nanoscale carriers as a potential platform for drug delivery and imaging. *Nat Mater*. 2010;9(2):172–178.
34. Chui SS, Lo SM, Charmant JP, Orpen AG, Williams ID. A chemically functionalizable nanoporous material. *Science*. 1999;283(5405):1148–1150.
35. Taylor-Pashow KM, Della Rocca J, Xie Z, Tran S, Lin W. Postsynthetic modifications of iron-carboxylate nanoscale metal-organic frameworks for imaging and drug delivery. *J Am Chem Soc*. 2009;131(40):14261–14263.
36. Wu YN, Zhou M, Li S, et al. Magnetic metal-organic frameworks: γ-Fe2O3@MOFs via confined in situ pyrolysis method for drug delivery. *Small*. 2014;10(14):2927–2936.
37. Moremen JR, Skopelja EN, Ceppa DP. The role of induction therapy. *J Thorac Dis*. 2014;6(Suppl 3):S309–S313.
38. Longley DB, Harkin DP, Johnston PG. 5-Fluorouracil: mechanisms of action and clinical strategies. *Nat Rev Cancer*. 2003;3(5):330–338.
39. Domvri K, Bougiouklis D, Zarogoulidis P, et al. Could somatostatin enhance the outcomes of chemotherapeutic treatment in SCLC? *J Cancer*. 2015;6(4):360–366.
40. Meyerhardt JA, Mayer RJ. Systemic therapy for colorectal cancer. *N Engl J Med*. 2005;352(5):476–487.
41. Yudi MB, Waksman R, Ajani AE. In-stent restenosis: local drug delivery with a stent or balloon. *J Thorac Dis*. 2015;7(10):1691–1692.
42. Toriumi F, Kubota T, Saikawa Y, et al. Thymidylate synthetase (TS) genotype and TS/dihydropyrimidine dehydrogenase mRNA level as an indicator in determining chemosensitivity to 5-fluorouracil in advanced gastric carcinoma. *Anticancer Res*. 2004;24(4):2455–2463.
43. Scalvini A, Ferrari V, Bodei S, et al. Involvement of target gene polymorphisms in 5-fluorouracil toxicity: a case report. *Pharmacology*. 2012;89(1–2):99–102.
44. Zhao D, Tan S, Yuan D, et al. Surface functionalization of porous coordination nanocages via click chemistry and their application in drug delivery. *Adv Mater*. 2011;23(1):90–93.
45. Yi H, Cho HJ, Cho SM, et al. Pharmacokinetic properties and antitumor efficacy of the 5-fluorouracil loaded PEG-hydrogel. *BMC Cancer*. 2010;10:211.
46. Costa P, Sousa Lobo JM. Modeling and comparison of dissolution profiles. *Eur J Pharm Sci*. 2001;13(2):123–133.
47. Siepmann J, Göpferich A. Mathematical modeling of bioerodible, polymeric drug delivery systems. *Adv Drug Deliv Rev*. 2001;48(2–3):229–247.
48. He C, Lu K, Lin W. Nanoscale metal-organic frameworks for real-time intracellular pH sensing in live cells. *J Am Chem Soc*. 2014;136(35):12253–12256.
49. He C, Lu K, Liu D, Lin W. Nanoscale metal-organic frameworks for the co-delivery of cisplatin and pooled siRNAs to enhance therapeutic efficacy in drug-resistant ovarian cancer cells. *J Am Chem Soc*. 2014;136(14):5181–5184.
50. Della Rocca J, Liu D, Lin W. Nanoscale metal-organic frameworks for biomedical imaging and drug delivery. *Acc Chem Res*. 2011;44(10):957–968.
51. Lee BR, Yu JY, Yoon SH, et al. Variability in the anti-tumor effect of tegafur-uracil depending on histologic types of lung cancer. *J Thorac Dis*. 2015;7(3):433–438.
52. Lucena FR, de Araújo LC, Rodrigues Mdo D, et al. Induction of cancer cell death by apoptosis and slow release of 5-fluoracil from metal-organic frameworks Cu-BTC. *Biomed Pharmacother*. 2013;67(8):707–713.
53. D'Journo XB, Thomas PA. Current management of esophageal cancer. *J Thorac Dis*. 2014;6 Suppl 2:S253–S264.
54. Zhang C, Zhou SS, Feng LY, et al. *In vitro* anti-cancer activity of chamaejasmenin B and neochamaejasmin C isolated from the root of *Stellera chamaejasme* L. *Acta Pharmacol Sin*. 2013;34(2):262–270.
55. Rong M, Chen G, Dang Y. Increased miR-221 expression in hepatocellular carcinoma tissues and its role in enhancing cell growth and inhibiting apoptosis in vitro. *BMC Cancer*. 2013;13:21.
56. Li S, Zheng L. Effect of combined treatment using wilfortrine and paclitaxel in liver cancer and related mechanism. *Med Sci Monit*. 2016;22:1109–1114.
57. Zhao YZ, Zhang L, Gupta PK, et al. Using PG-liposome-based system to enhance puerarin liver-targeted therapy for alcohol-induced liver disease. *AAPS PharmSciTech*. 2016;17(6):1376–1382.
58. Ren F, Yang B, Cai J, Jiang Y, Xu J, Wang S. Toxic effect of zinc nanoscale metal-organic frameworks on rat pheochromocytoma (PC12) cells in vitro. *J Hazard Mater*. 2014;271:283–291.